

Analysis of binding mode of vibsandin A with protein kinase C C1 domains: An experimental and molecular dynamics simulation study

Ryo C. Yanagita^{a,*}, Mao Otani^a, Satoshi Hatanaka^a, Hiroto Nishi^a, Shota Miyake^a, Yusuke Hanaki^a, Masashi Sato^a, Yasuhiro Kawanami^a, and Kazuhiro Irie^b

^aDepartment of Applied Biological Science, Faculty of Agriculture, Kagawa University, Kagawa 761-0795, Japan

^bDivision of Food Science and Biotechnology, Graduate School of Agriculture, Kyoto University, Kyoto 606-8502, Japan

Corresponding Author

*(R.C.Y.) E-mail: yanagita.ryo@kagawa-u.ac.jp

ORCID 

Ryo C. Yanagita: 0000-0002-9217-5507



This is an Accepted Manuscript version of the following article, accepted for publication in *Journal of Molecular Structure*.

Analysis of binding mode of vibsandin A with protein kinase C C1 domains: An experimental and molecular dynamics simulation study

Ryo C. Yanagita, Mao Otani, Satoshi Hatanaka, Hiroto Nishi, Shota Miyake, Yusuke Hanaki, Masashi Sato, Yasuhiro Kawanami, Kazuhiro Irie

Journal of Molecular Structure, 2022, Article number 132866.

<https://doi.org/10.1016/j.molstruc.2022.132866>

It is deposited under the terms of the Creative Commons Attribution-NonCommercial-NoDerivatives License (<http://creativecommons.org/licenses/by-nc-nd/4.0/>), which permits non-commercial re-use, distribution, and reproduction in any medium, provided the original work is properly cited, and is not altered, transformed, or built upon in any way.

Keywords: Protein kinase C; C1 domain; Vibsandin A; CH–O hydrogen bond; Structure–activity study

Abbreviations: PKC, protein kinase C; DAG, 1,2-diacyl-*sn*-glycerol; TPA, 12-*O*-tetradecanoylphorbol 13-acetate; VibA, vibsandin A; VibB, vibsandin B; Epoxy-VibB, epoxyvibsandin B; PDBu, phorbol 12,13-dibutyrate; K_d , dissociation constant; K_i , binding inhibition constant; MD, molecular dynamics; MM-PBSA, Molecular Mechanics/Poisson–Boltzmann Surface Area

ABSTRACT

Vibsanin A (VibA), isolated from *Viburnum odoratissimum*, binds to and activates protein kinase C (PKC) isozymes to induce leukemia cell differentiation. VibA is a promising seed compound for developing PKC-activating drugs because it exhibits anti-proinflammatory activity, atypical to PKC activators. However, the role of hydrogen bond-forming functional groups and the precise binding mode with C1 domains in PKC isozymes remains unknown. In this study, we evaluated the PKC-binding ability of natural vibsanins and synthetic 1'-desoxy-VibA (**1**) and performed molecular dynamics simulation of membrane/C1 domain-bound VibA to predict the binding mode of VibA with C1 domains. Experimental and simulation results indicated that the ester group in VibA is involved in CH–O hydrogen bonds with PKC C1 domains. Alternatively, a growth-inhibition assay against leukemia cells revealed that the ester group of VibA negatively affects antiproliferative activity.

1 INTRODUCTION

Protein kinase C (PKC) is a family of serine/threonine-specific kinases involved in several cellular functions, including proliferation, apoptosis, and tumorigenesis.¹⁻³ Over the years, the PKC family has attracted attention as a potential therapeutic target for cancer, Alzheimer's disease, and human immunodeficiency virus infection.³ In humans, it is composed of at least ten isozymes, which differ in phylogeny and biochemistry, resulting in further classification into three subfamilies: calcium-dependent conventional PKCs (α , β I, β II, γ), calcium-independent novel PKCs (δ , ϵ , η , θ), and atypical PKCs (ζ , λ /i).³ 1,2-Diacyl-sn-glycerol (DAG), a second-messenger, binds to tandem C1 domains (C1A and C1B) in the regulatory region of conventional and novel PKCs, activating these isozymes. By mimicking DAG, naturally-occurring PKC ligands such as 12-O-tetradecanoylphorbol 13-acetate (TPA) and bryostatin-1 (Figure 1) bind to C1 domains and act as PKC agonists.⁴⁻⁶ Recently, the U.S. Food and Drug Administration has approved two natural PKC ligands as drugs: Ingenol mebutate (Figure 1) as a topical gel for treating actinic keratosis, which is a pre-cancerous skin lesion,⁷ and tigilanol tiglate with a phorbol skeleton for treating mast cell tumors in dogs.⁸ However, strong tumor-promoting and proinflammatory effects, having acute adverse effects and hampering oral and intravenous administrations, have limited clinical use of most PKC ligands. Therefore, the discovery and development of non-tumor-promoting and non-proinflammatory PKC ligands have been a long-standing goal in this field.

Recently, vibsanin A (VibA), an eleven-membered diterpenoid isolated from leaves of *Viburnum odoratissimum* in 1980,⁹⁻¹¹ has been discovered as a new PKC ligand.¹² It was striking that VibA induced leukemia cell differentiation and suppressed TPA-induced inflammation on mouse skin,¹² indicating VibA as a potential seed for developing PKC-activating drugs without tumor-promoting activity. However, to rationally design derivatives or analogs of VibA, we need to know or predict the accurate binding mode of VibA with C1 domains of PKCs. Yu *et al.* reported that the oxidation of position 5 of VibA decreased its differentiation induction activity.¹² Matsuki *et al.* also reported that the 18-OH group of VibA is critical for the cell differentiating activity,¹³ which is consistent with the structure-activity relationship studies on other classes of PKC ligands, including phorbol esters,¹⁴ ingenol esters,¹⁵ teleocidins,¹⁶ and aplysiatoxins¹⁷ (Figure 1). However, the role of VibA's 6,7-epoxy and 1'-ester-carbonyl groups in binding to C1 domains is unknown.

In this report, we describe the ability to bind to PKC α and δ isozymes, as well as isolated PKC α -C1A, α -C1B, δ -C1A, and δ -C1B domains and antiproliferative activity of VibA, vibsanin B (VibB), vibsanol C, epoxyvibsanin B (epoxy-VibB), and synthetic 1'-desoxovibsanin A (**1**, Figure 2), implying that both the epoxy and ester-carbonyl groups play vital roles in the strong affinity to C1 domains. In addition, MD simulation of PKC δ -C1B domain in complex with VibA in the phospholipid bilayer suggested that the epoxy group forms a relatively strong hydrogen bond with an NH group of Gly-253 of PKC δ -C1B, and

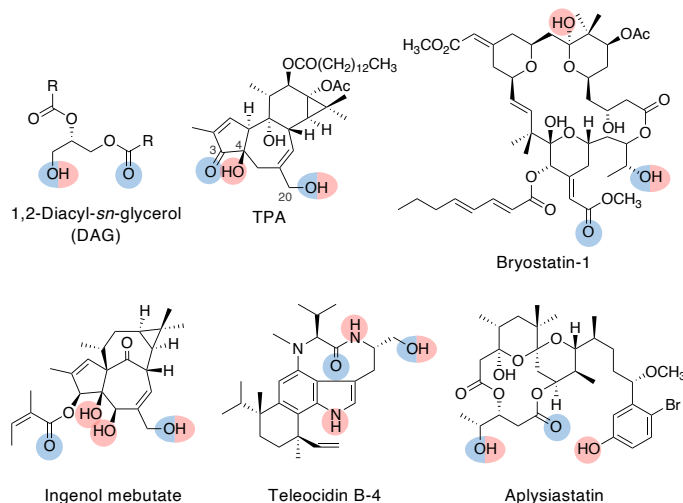


Figure 1: Structures of naturally-occurring protein kinase C (PKC) ligands. Red and blue circles behind the structure diagrams represent hydrogen bond donors and acceptors involved in binding to PKC, respectively.

the 1'-carbonyl group occasionally forms a weaker hydrogen bond with the same NH group but primarily forms a CH-O hydrogen bond with an H α atom of Gly-253.

2 RESULTS AND DISCUSSION

2.0.1 Isolation of vibsanins and synthesis of 1'-desoxovibsanin A (1)

VibA, vibsanol C,¹⁸ VibB,^{9,19} and epoxy-VibB²⁰ were isolated from *Viburnum odoratissimum* according to the previously described procedures.⁹ Nuclear magnetic resonance (NMR) signals of epoxy-VibB were assigned using two-dimensional NMR techniques (Table 1), which are nearly consistent with ¹H NMR data in the literature²⁰ (Supplementary materials, Table S1).

Because the ester group at position 8 is a common moiety among eleven-membered vibsanins, we cannot assess the role of the carbonyl group at position 1' by comparing the natural vibsanins. Therefore, we synthesized and evaluated the biological activities of 1'-desoxovibsanin A (1), as shown in Scheme 1, with an overall yield of 19% in four steps.

2.1 The ability of VibA to bind to PKC α and δ isozymes, and their C1 domains

Recently, Hanaki *et al.* have reported that, among PKC isozymes, PKC α and δ isozymes are predominantly expressed in cancer cell lines and are involved in the antiproliferative activity of the simplified analog of aplysiatoxin.²¹ Thus, we first evaluated the binding ability of VibA for recombinant human PKC α and δ isozymes using a competitive binding assay with tritium-labeled phorbol 12,13-dibutyrate ([³H]PDBu)

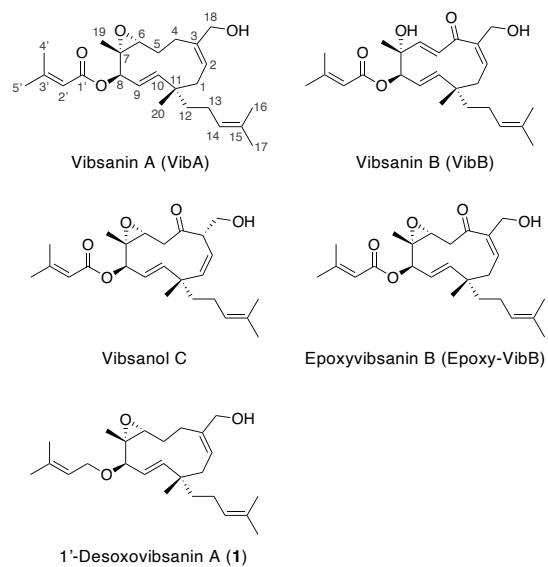
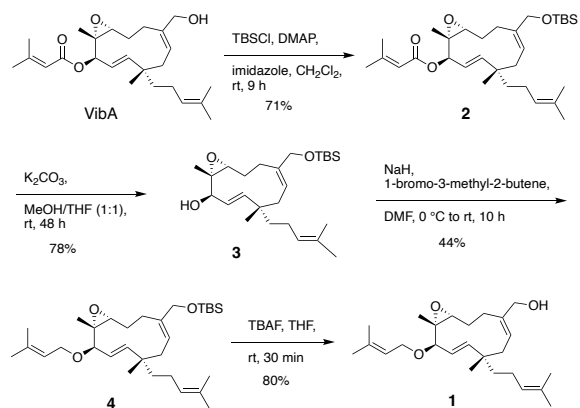


Figure 2: Structures of natural vibsantin congeners and 1'-desoxovibsantin A (1).



Scheme 1. Synthesis of 1'-desoxovibsantin A (1).

Table 1: ^1H and ^{13}C NMR data for epoxyvibsanin B in CDCl_3 , 297 K (600 MHz for ^1H and 150 MHz for ^{13}C).

No.	Epoxyvibsanin B			
	δH (ppm)	mult.	J (Hz)	δC (ppm)
1 α	2.62	dd	12.2, 6.4	40.2
1 β	1.97	dd	12.2, 11.0	-
2	5.76	dd	11.0, 6.4	130.5
3	-			145.8
4	-			203.8
5 α	2.74	dd	17.8, 10.7	40.5
5 β	3.21	dd	17.8, 4.3	-
6	3.39	dd	10.7, 4.3	59.3
7	-			60.3
8	5.08	d	9.7	77.2
9	5.33	dd	15.9, 9.7	122.4
10	5.69	d	15.9	145.8
11	-			40.3
12a	1.27	ddd	13.2, 12.0, 5.5	38.9
12b	1.50	ddd	13.2, 12.2, 4.6	-
13a	1.78	m		23.1
13b	1.90	m		-
14	5.05	t sep ^a	7.0, 1.2	124.3
15	-			131.6
16	1.57	s		17.6
17	1.66	s		25.7
18a	4.18	dd	12.9, 2.9	64.6
18b	4.50	dd	12.9, 8.0	-
19	1.45	s		17.5
20	1.05	s		23.5
1'	-			165.3
2'	5.61	br s		115.9
3'	-			157.4
4'	2.15	d	1.2	20.3
5'	1.90	d	1.2	27.4

^a Triplet of septets.

based on the method of Sharkey and Blumberg²² with minor modifications. Figure 3 shows a decrease in the [³H]PDBu binding ratio with increasing VibA concentration. Apparent binding inhibition constants (K_i) of VibA, corresponding to a dissociation constant K_d , calculated from its IC_{50} values for PKC α and δ were 12 and 14 nM (Table 2), respectively, indicating that VibA has little selectivity between the two isozymes. However, the relatively slow rate of the decrease in the [³H]PDBu binding ratio with increasing VibA concentration and the biphasic nature of the binding inhibition trend in PKC δ indicate that VibA has significant binding selectivity between C1A and C1B domains in both PKC α and δ compared to [³H]PDBu.

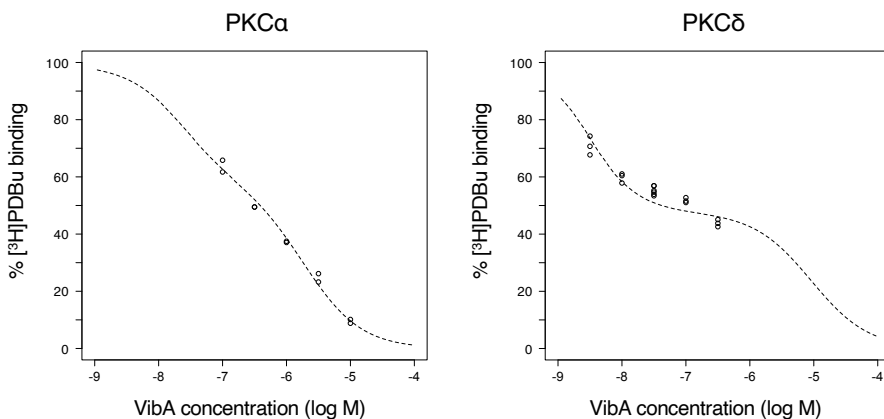


Figure 3: Binding of VibA for recombinant human PKC α and δ . Binding assay was performed with a fixed [³H]PDBu concentration (~ 12.6 nM). Curved dashed lines represent theoretical binding inhibition curves using the K_i values of VibA for each binding site, estimated by nonlinear regression analysis.

Table 2: K_i values of VibA for PKC α and δ isozymes, and synthetic C1 peptides.

PKC isozymes and C1 peptides	K_i (nM) of VibA	K_d (nM) of [³ H]PDBu ^a
PKC α	12	0.46
α -C1A	1100 ^b (600–2100) ^c	1.1
α -C1B	42 (22–81) ^c	5.3
PKC δ	14	0.76
δ -C1A	1400 (900–2300) ^c	52
δ -C1B	0.28 (0.12–0.65) ^c	0.53

^a Cited from Ref. 23. ^b Mean values from two independent experiments (triplicate for each ligand concentration). ^c 95% confidence interval.

We performed the binding assay using synthetic C1 peptides²³ as surrogates of isolated C1 domains to accurately evaluate the affinity of VibA for each C1 domain. These peptides can be correctly folded *in vitro* by zinc ions and appropriate pH adjustment and exhibit comparable affinity to PKC ligands as recombinant enzymes.²⁴ The K_i values of VibA for synthetic α -C1A, α -C1B, δ -C1A, and δ -C1B peptides were 1100, 42, 1400, and 0.28 nM (Table 2), respectively. The binding inhibition curves are presented in

the Supplementary materials. The comparison with K_d values of [^3H]PDBu (Table 2) suggests that VibA has binding selectivity for C1B domains, especially for ones in novel PKC isozymes. The K_i value of VibA for δ -C1B was comparable to those of naturally-occurring tumor promoters: aplysiatoxin (K_i , 0.41 nM)²⁵ and teleocidin B-4 (K_i , 0.12 nM; 95% CI, 0.0055–2.5). Conversely, the affinity of VibA for α -C1A was relatively lower: approximately 4,000 times lower than that for δ -C1B and approximately 3,000 times lower than that of aplysiatoxin for α -C1A (K_i , 0.40 nM).²⁵ The degree of binding selectivity of VibA for δ -C1B was the highest among known natural and synthetic PKC ligands: The most novel PKC-selective ligand known was 1-hexylindolactam-V10, a ten-membered teleocidin analog, showing approximately 450-fold selectivity for δ -C1B over α -C1A.²⁶ Regarding teleocidin analogs, expanding the size of a lactam ring from eight to nine or nine to ten made the ring more flexible, increasing binding selectivity for novel PKC C1B domains.^{26–28} Therefore, the relatively high binding selectivity of VibA may be attributable to its flexible eleven-membered ring structure.

Since the C1A domain in PKC α and the C1B domain in PKC δ are the primary binding sites of tumor promoters,²⁴ binding abilities of the other vibsansins and **1** were evaluated using α -C1A and δ -C1B peptides.

Table 3: K_i values of VibB, Vibsanol C, Epoxy-VibB, and **1** for the PKC α -C1A and δ -C1B peptides

PKC C1 peptides	K_i (nM)			
	VibB	Vibsanol C	Epoxy-VibB	1
α -C1A	NB ^a	NB	NB	1800 ^b (71–43,000) ^c
δ -C1B	230 (48–1100) ^c	50 (24–110) ^c	75 (2–2900) ^c	3.3 (0.3–34) ^c

^a No binding at maximum assay concentration ($10^{-4.5}$ M) ^b Mean values from two independent experiments (triplicate for each ligand concentration). ^c 95% confidence interval.

2.2 The ability of vibsansins and **1** to bind to PKC C1 domains

Table 3 presents the K_i values of other vibsansins and **1**. The binding inhibition curves are presented in the Supplementary materials. The binding ability of VibB (K_i , 230 nM), vibsanol C (K_i , 50 nM), and epoxy-VibB (K_i , 75 nM) for δ -C1B was approximately 170–800 times lower than that of VibA (K_i , 0.28 nM), and these compounds showed no binding ability for α -C1A at maximum assay concentration ($10^{-4.5}$ M). These results imply that the carbonyl group at position 4 interferes with the binding of ligands to the C1 domain, which is consistent with the report that, unlike VibA, VibB and structurally-related vibsansin L with a 4-oxo group did not induce HL-60 cell differentiation.¹² Note that PKC β mediates the differentiation of HL-60 cells induced by PKC ligands,²⁹ and C1 domain sequences of PKC α and β are almost identical. Comparing VibB, vibsanol C, and epoxy-VibB, the ability of vibsanol C and epoxy-VibB was slightly higher than that of VibB, indicating the importance of the epoxy group in binding to the C1 domain.

The binding ability of **1** without a carbonyl group at position 1' for δ -C1B (K_i , 3.3 nM) was approximately 12 times lower than that of VibA, which corresponds to the 1.35 kcal mol⁻¹ difference in the binding free energy (calculated at 277.15 K). The free energy of hydrogen bond formation ranges from 1.5 to 4.7 kcal mol⁻¹, and removing a hydrogen bond acceptor of PKC ligands significantly reduces affinity.^{17,30} For example, removing the carbonyl oxygen atom in a lactone ring of DAG-lactones resulted in approximately 200–2,000 times reduction of affinity for the PKC δ -C1B domain.³⁰ Therefore, the approximately 12 times lower affinity of **1** than VibA implies that the carbonyl group at position 1' of VibA is involved in a weak hydrogen bonding with δ -C1B.

2.3 Molecular modeling study

To predict the binding mode of VibA with the PKC C1 domains and investigate the role of the carbonyl group at position 1', we performed docking simulation and all-atom MD simulation of VibA and **1** in phospholipid bilayer environment, as previously described.³¹ We used the predicted three-dimensional structure of the PKC α -C1A domain, built by homology modeling, and the crystal structure of the PKC δ -C1B domain¹⁴ (PDB code: 1PTR) for the simulations. Based on the simulation trajectory, we analyzed the binding mode and intermolecular hydrogen bonding network. The binding free energy, $\Delta G_{\text{bind}}^{\circ}$, was predicted by combining molecular mechanics Poisson-Boltzmann surface area (MM-PBSA) energy and the free energy of transfer calculated using the PPM server, as previously described.³¹ The MM-PBSA method is a feasible approach to estimate the free energy of binding in an aqueous solution. However, because we cannot directly apply this method to a membrane/protein/ligand dynamical system, we combined it with the empirically calculated free energy of membrane transfer.

Figure 4A and 4C show the major binding modes of VibA with the PKC α -C1A and PKC δ -C1B domains in the MD simulation. These major binding modes shared a hydrogen-bonding network involving the binding cleft-forming Gly, Leu/Ile, and Thr residues. VibA formed three hydrogen bonds between the 6,7-epoxy and NH groups of Gly-59 (PKC α -C1A) or Gly-253 (PKC δ -C1B), the 18-OH and C=O groups of Ile-57 (PKC α -C1A) or Leu-251 (PKC δ -C1B), and the 18-OH and NH groups of Thr-48 (PKC α -C1A) or Thr-242 (PKC δ -C1B). These hydrogen bonding groups in the protein side are involved in the binding of PKC ligands.^{15-17,32} For example, in phorbol esters, the 3-C=O group forms a hydrogen bond with Gly-253, and the 20-OH group forms hydrogen bonds with Thr-242 and Leu-251 (PDB ID: 1PTR; Figure 4E).^{14,15}

The 1'-ester-carbonyl group formed a CH-O hydrogen bond³³ with an H α atom of the Gly-253 residue in the major binding modes. In addition, H-8 of VibA formed another CH-O hydrogen bond with the C=O group of the Gly residue, which has geometrical similarity to a hydrogen bond between 4-OH of a phorbol ester and the C=O group of the Gly-253 (Figure 4E).¹⁴ A CH-O hydrogen bond is weaker than a conventional hydrogen bond even though it significantly contributes to the protein structure, nucleic acid structure, and molecular recognition.³³

In the minor mode with the PKC α -C1A domain (Figure 4B), the 1'-carbonyl group did not have interaction with Gly-59 due to the steric hindrance with Phe-60, a residue existing in PKC α -, β - and η -C1A domains. On the other hand, in the minor mode with the PKC δ -C1B domain (Figure 4D), the 1'-carbonyl and 6,7-epoxy groups occasionally and simultaneously formed hydrogen bonds with the NH group of Gly-253 (Figure 4B), known as bifurcated hydrogen bonds or, specifically, two-acceptor/one-donor bifurcated hydrogen bonds. However, the occurrence and importance of this type of hydrogen bond are insignificant.³⁴

Figure 5 shows distribution histograms of interatomic length between a hydrogen atom and an acceptor atom involved in each hydrogen bond. Percentages shown in each panel represent the probability of the presence of each hydrogen bond. The criteria used was that a distance between a hydrogen atom and an acceptor atom must be equal to or less than 2.7 Å, which is less than the sum of van der Waals radii of hydrogen (1.20 Å) and oxygen (1.52 Å) atoms. The histograms show that the hydrogen bonds involving the OH and epoxy groups of VibA stably existed in the simulation. On the other hand, the 1'-carbonyl group formed a hydrogen bond only 5.7% and 2.2% of the simulation time for PKC α -C1A and PKC δ -C1B, respectively, implying that the binding mode with the bifurcate hydrogen bond (Figure 4D) is rare and does not significantly contribute to the binding of VibA. The distance distributions of the CH-O hydrogen bonds suggest that the 1'-carbonyl group and the H-8 of VibA formed CH-O hydrogen bonds with the proteins, though PKC δ -C1B is more likely to form those interactions than PKC α -C1A.

Table 4 presents the predicted and experimental $\Delta G_{\text{bind}}^{\circ}$ of VibA and **1** for α -C1A and δ -C1B and their energy components in the MM-PBSA calculation. Comparing VibA- α -C1A and VibA- δ -C1B, the difference in predicted $\Delta G_{\text{bind}}^{\circ}$ ($\Delta\Delta G_{\text{bind}}^{\circ}$, 4.3 kcal mol⁻¹) was roughly consistent with the experimen-

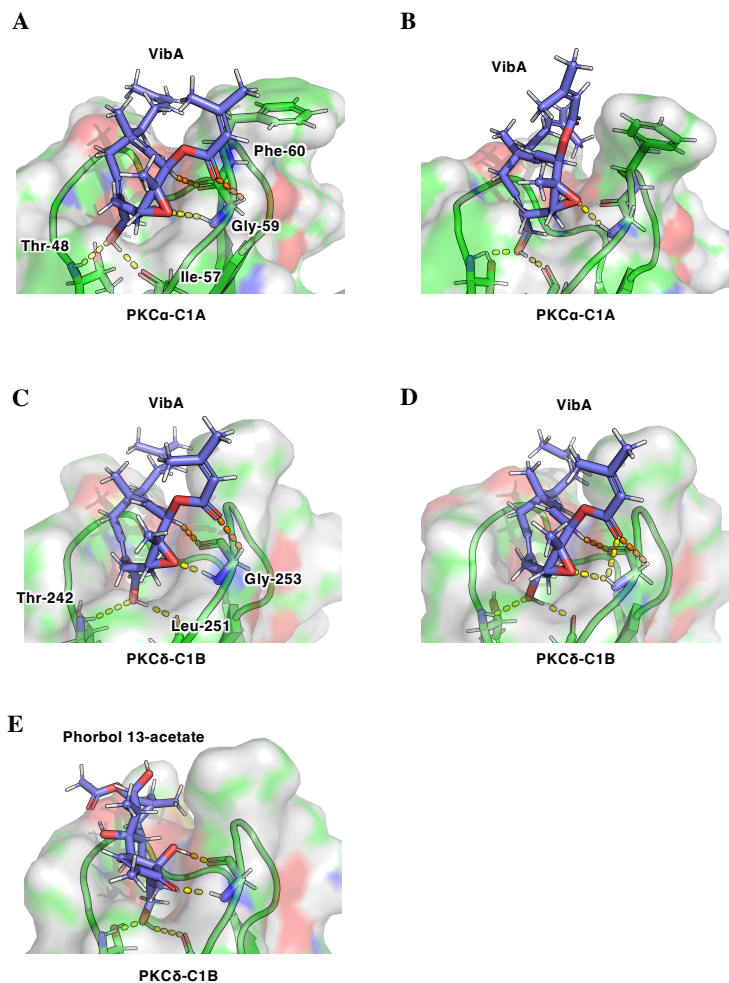
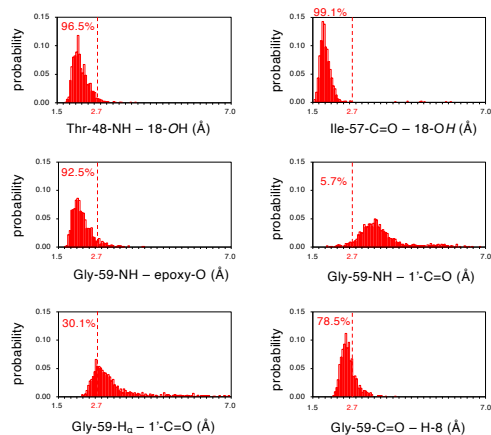


Figure 4: Typical binding modes of VibA with the PKC α -C1A (panels A and B) and PKC δ -C1B (panels C and D) domains in the MD simulation and an experimental binding mode of phorbol 13-acetate (panel E). A) The major binding mode of VibA with the PKC α -C1A domain in which the 1'-carbonyl group of VibA forms a CH-O hydrogen bond with an H α atom of Gly-59. B) The minor binding mode of VibA with the PKC α -C1A domain in which the 1'-carbonyl and the epoxy groups do not interact with the Gly-59 residue. C) The major binding mode of VibA with the PKC δ -C1B domain in which the 1'-carbonyl group of VibA forms a CH-O hydrogen bond with an H α atom of Gly-253. D) The minor binding mode of VibA with the PKC δ -C1B domain in which the 1'-carbonyl group and the epoxy group forms bifurcated hydrogen bonds with the NH group of Gly-253. E) The binding mode of phorbol 13-acetate with the PKC δ -C1B domain (PDB ID: 1PTR), where hydrogen atoms are added and energetically minimized. VibA, Thr-48, Ile-57, Phe-60, Gly-59, Thr-242, Leu-251, and Gly-253 are shown in the stick model. Hydrogen, oxygen, and nitrogen atoms are colored white, red, and blue. Carbon atoms are colored either green (for protein) or violet (for VibA). A solvent-accessible surface is shown for the protein.

A PKC α -C1A



B PKC δ -C1B

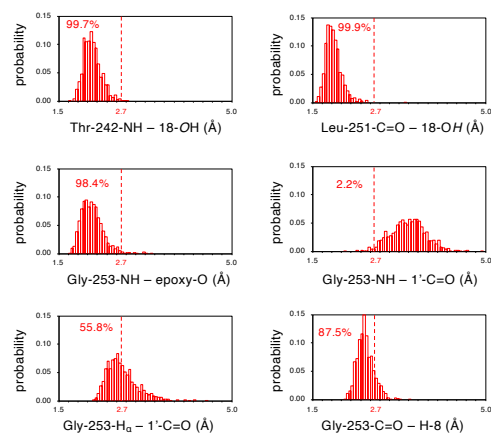


Figure 5: Histograms for lengths of intermolecular hydrogen bonds between the A) PKC α C1A and VibA, and B) PKC δ C1B and VibA in the MD simulation. Bin width is 0.05 Å. Each box shows the probability for the presence of the hydrogen bond (criteria, ≤ 2.7 Å).

Table 4: Predicted and experimental $\Delta G_{\text{bind}}^{\circ}$ (kcal mol⁻¹) of VibA and **1** for the PKC α C1A and PKC δ C1B domains and energy components in the MM-PBSA calculation.

	PKC α -C1A		PKC δ -C1B	
	VibA	1	VibA	1
$\Delta E_{\text{MM-PBSA}}$ (A)	-7.7439	-7.2741	-11.9874	-11.0459
van der Waals	-32.3066	-31.5354	-33.1619	-33.0092
electrostatic	-25.1940	-17.9207	-26.4170	-19.1333
polar solvation	35.4879	27.7750	34.3138	27.7063
nonpolar solvation	-24.0990	-23.7672	-24.3424	-24.3623
dispersion	38.3625	38.1793	37.6206	37.7642
$\Delta G_{\text{transfer}}$ (B) ^a	-11.2	-11.8	-11.2	-12.0
predicted $\Delta G_{\text{bind}}^{\circ}$ (A+B)	-18.9	-19.1	-23.2	-23.0
experimental $\Delta G_{\text{bind}}^{\circ}$ ^b	-8.45	-8.15	-13.5	-12.0

^a Calculated using the PPM server and program.³⁵ ^b Experimental $\Delta G_{\text{bind}}^{\circ} = (1/4184) \times -RT \ln(C^{\circ} K_i^{-1})$, where R represents the gas constant (8.31446 J/K/mol), $T = 310$ (K), and C° represents the standard concentration (1 M).

tal ($\Delta \Delta G_{\text{bind}}^{\circ}$ (5.05 kcal mol⁻¹). All MM-PBSA energy terms for VibA- α -C1A were slightly greater than those for VibA- δ -C1B. Also, there was no significant difference in the results of energy decomposition per residue (Figure 6) between VibA- α -C1A and VibA- δ -C1B. These results suggest that the significantly lower affinity of VibA for α -C1A is not attributable to loss of specific interaction types or specific residues.

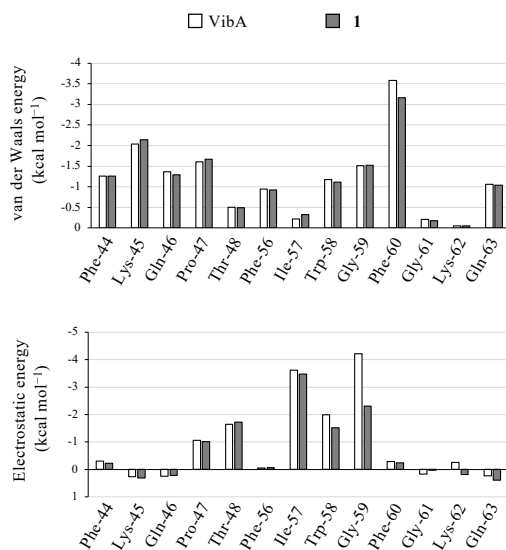
Comparing VibA and **1**, $\Delta E_{\text{MM-PBSA}}$ for VibA was approximately 0.5 and 0.9 kcal mol⁻¹ less than that for **1** in α -C1A and δ -C1B, respectively. Compared with VibA, attractive electrostatic energy decreased by -7.3 kcal mol⁻¹ in **1**, and the decrease in positive polar solvation energy term (7.7 and 6.6 kcal mol⁻¹) did not fully compensate for this decrease. The energy decomposition per residue indicated that, while the van der Waals energy per residue did not differ between VibA and **1**, the attractive electrostatic energy with Gly-59 or Gly-253 decreased by approximately 2 kcal mol⁻¹ in **1** compared with VibA (Figure 6). Alternatively, the existence of a carbonyl group at position 1' doubled the attractive electrostatic interaction with the Gly residue. This change in the electrostatic energy component can be attributed to the loss of the CH-O hydrogen bond involving the 1'-carbonyl group and the decrease in the acidity of H-8 of VibA that forms CH-O hydrogen bond with the C=O group of the Gly residue. The experimental energy of a CH-O hydrogen bond formation is 1 kcal mol⁻¹,³³ which can explain the decrease in the binding ability of **1** (1.35 kcal mol⁻¹).

2.4 The antiproliferative activity of VibA and **1** against MOLT-4F leukemia cell line

To examine the effect of removing the 1'-carbonyl group on the antiproliferative activity, we conducted a growth-inhibition test against a human acute T lymphoblastic MOLT-4F cell line. Drexler *et al.* reported that TPA inhibited the proliferation of the MOLT-4 cell line, a parent cell line of MOLT-4F cells.³⁶ MOLT-4F cells were treated with VibA or **1** and incubated for 48 h, and then cell viability was measured by cell counting kit-8 (Dojindo). GI_{50} , the concentration required for 50% growth-inhibition, calculated from the growth-inhibition curve, represents the antiproliferative activity of the compounds.

The GI_{50} of VibA and **1** against MOLT-4F cells were 3.4 and 0.72 μ M, respectively (Table 5); VibA exhibited approximately 5-fold lower antiproliferative activity than **1**. Because the molecular hydropho-

A PKC α -C1A



B PKC δ -C1B

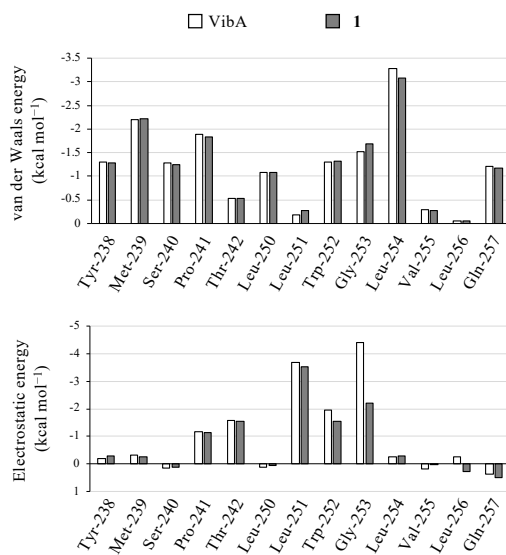


Figure 6: Decomposition of van der Waals and electrostatic energies from the MD simulation between VibA or 1 and the A) PKC α C1A or B) PKC δ C1B domain per residue. Values for residues that form ligand-binding cleft are shown.

bicities (ClogP) of VibA and **1** are almost equal (Table 5), the discrepancy between their binding ability to PKC C1 domains and antiproliferative activity against MOLT-4F cells cannot be attributed to their difference in membrane permeability or cellular uptake.

Table 5: GI₅₀ values for MOLT-4F cells, half-lives ($t_{1/2}$) in phosphate-buffered saline, and ClogP values of VibA and **1**.

	VibA	1
GI ₅₀ (μ M) for MOLT-4F cells	3.4 (0.5) ^a	0.72 (0.21) ^a
$t_{1/2}$ (h)	20.0 (0.2) ^a	10.7 (0.1) ^a
ClogP ^b	6.51	6.52

^a Standard deviation from two or three independent experiments. ^b Calculated by ChemDraw 20.0.

2.5 Stability of VibA and **1** in an aqueous buffer

To investigate why VibA exhibited lower antiproliferative activity than **1**, we conducted a chemical stability test for VibA and **1** in phosphate-buffered saline (PBS) at 37 °C. We measured the residual amounts of VibA and **1** by reversed-phase HPLC and calculated the half-life ($t_{1/2}$) for each compound. The half-lives ($t_{1/2}$) of VibA and **1** in the PBS solution at 37 °C were 20.0 and 10.7 h, respectively (Table 5). As a result, we cannot explain the lower antiproliferative activity of VibA in terms of chemical stability.

In a liquid chromatography/time-of-flight mass spectrometry (LC-TOF-MS) analysis of VibA in the PBS solution, we detected oxidation products with a formula C₂₅H₃₆O₅ (observed m/z 439.2461, calculated 439.2460 for C₂₅H₃₆O₅Na) and different retention times but no hydrolytic product from the hydrolysis of an ester group at position 8. We also found that VibA rapidly decomposed in a methanol-diluted PBS solution, even when stored on ice, within an hour. These results imply that oxidation is a primary cause of the degradation of VibA in an aqueous buffer. Therefore, the lower activity of VibA than **1** might be attributed to VibA’s susceptibility to oxidation, which decreases molecular hydrophobicity and introduces a steric hindrance with the receptor, degrading VibA’s biological activity.

3 Conclusion

In this study, through the structure–activity relationship investigation and molecular dynamics simulation, we examine the role of polar functional groups of VibA in its biological activity. The experimental and simulation results suggested that the 6,7-epoxy and 1'-carbonyl groups of VibA form a conventional hydrogen bond and a CH–O hydrogen bond, respectively, with Gly-59/253 of the PKC α C1A/PKC δ C1B domains, that is, a conserved residue in the C1 domain family. The simulation results also suggested that the existence of an electron-withdrawing ester group at position 8 strengthens the CH–O hydrogen bond between H-8 of VibA and the C=O of Gly-59/253.

Comparison of binding ability to PKC C1 domains, growth-inhibitory activity against MOLT-4F cells, and chemical stability of VibA and **1** revealed that the ester side-chain in VibA favors binding to PKC but negatively affects the antiproliferative activity, which is presumably due to its susceptibility to oxidation and hydrolysis, which causes a loss of molecular hydrophobicity. Furthermore, because prolonged activation and subsequent degradation of PKC isozymes could be involved in the tumor-promoting activity of PKC ligands, the relatively unstable nature of VibA might be a key for its unique anti-proinflammatory activity on mouse skin.¹²

So far, CH/ π interactions have garnered attention in the development of analogs of naturally-occurring PKC ligands,^{26,37,38} whereas CH–O hydrogen bonds have not. The prediction that CH–O hydrogen bonds play a substantial role in the binding of VibA provided new insight into the molecular recognition by C1 domains, which will help design artificial analogs of PKC ligands with higher affinity.

4 Experimental

4.1 General remarks

The following spectroscopic and analytical instruments were used: Digital Polarimeter, Jasco P-1010 (JASCO, Tokyo, Japan); ¹H and ¹³C, JOEL JNM-ECA 600 and JEOL JNM-ECZ500 (JEOL, Japan; reference, TMS); microplate reader, Multiskan FC (Thermo SCIENTIFIC); HPLC, JASCO PU-980 Intelligent HPLC pump with a JASCO PV-970 Intelligent UV/VIS Detector and JASCO PU-4086 Semi-preparative Pump with a JASCO UV-4075 UV/VIS Detector (JASCO, Tokyo, Japan); MPLC, EPCLC-AI-580S (Yamazen, Osaka, Japan); HR-ESI-TOF-MS, Xevo G2-XS (Waters, Tokyo, Japan) equipped with an ACQUITY UPLC BEH C18 column (Waters, Tokyo, Japan). HPLC was carried out on YMC-Pack ODS-AM AM12S05-2510WT, ODS-A AA12S05-1006WT, SIL SL12S05-1510WT, and SIL SL12S16-1520WT (YMC, Kyoto, Japan). Wakogel C-300 (silica gel, FUJIFILM Wako Pure Chemical Corporation, Osaka, Japan), activated charcoal powder (FUJIFILM Wako Pure Chemical Corporation), and Sephadex LH-20 (GE Healthcare Japan) were used for open and flash column chromatography. [³H]PDBu (17.16 Ci mmol⁻¹) was custom-synthesized by PerkinElmer Life Science Research Products (Boston, MA, US). Poly(ethylene glycol) 8000 and bovine γ -globulin were purchased from Sigma-Aldrich. 1,2-Dioleoyl-*sn*-glycero-3-phospho-L-serine (sodium salt, chloroform solution) was purchased from Funakoshi (Tokyo, Japan). Recombinant human PKC α and PKC δ were purchased from ThermoFisher Scientific (Waltham, MA, USA). The PKC C1 peptides were synthesized as reported previously.²³ RPMI-1640 medium with L-Glutamine, phenol red and HEPES, glucose-free RPMI-1640, Penicillin-Streptomycin, and Cell Counting Kit-8 (DOJINDO) were purchased from Wako Pure Chemical Corporation. Fetal Bovine Serum was purchased from Equitech Bio. All other chemicals and reagents were purchased from chemical companies and used without further purification.

4.2 Isolation of vibsanins

Vibsanin A and vibsanol C were isolated from leaves of *V. odoratissimum*, which were collected in Kagawa, Japan, based on the procedure of Kawazu.⁹ Vibsanin B and epoxyvibsanin B was isolated from flower buds of *V. odoratissimum*, which were collected in Kagawa, Japan, based on the same procedure. Before use, we purified these natural products by reversed-phase high-performance liquid chromatography (HPLC), silica gel HPLC, or both.

Vibsanin A was purified by reversed-phase HPLC (column, YMC-Pack ODS-AM AM12S05-1520WT; solvent, 85% MeOH/H₂O; flow rate, 8.0 mL min⁻¹; UV detection, 220 nm and 254 nm; retention time, 19.0 min).

Vibsanol C was purified by reversed-phase HPLC (column, YMC-Pack ODS-AM AM12S05-1520WT; solvent, 85% MeOH/H₂O; flow rate, 8.0 mL min⁻¹; UV detection, 220 nm and 254 nm; retention time, 14.7 min) followed by silica gel HPLC (column, YMC-Pack SIL SL12S05-1510WT; solvent, 35% EtOAc/hexane; flow rate, 3.0 mL min⁻¹; UV detection, 220 nm and 254 nm; retention time, 10.3 min). In ¹H-1D NMR spectrum of vibsanol C, signals from major and minor conformers were observed for protons at positions 18 and 18-OH (Supplementary data, Table S2).

Vibsanin B was purified by reversed-phase HPLC (column, YMC-Pack ODS-AM AM12S05-1520WT; solvent, 85% MeOH/H₂O; flow rate, 8.0 mL min⁻¹; UV detection, 220 nm and 254 nm; retention time, 10.3 min) followed by silica gel HPLC (column, YMC-Pack SIL SL12S05-1510WT; solvent, 50% EtOAc/hexane; flow rate, 3.0 mL min⁻¹; UV detection, 254 nm; retention time, 9.5 min).

Epoxyvibsanin B was purified by reversed-phase HPLC (column, YMC-Pack ODS-AM AM12S05-1520WT; solvent, 85% MeOH/H₂O; flow rate, 8.0 mL min⁻¹; UV detector, 220 nm and 254 nm; retention time, 12.6 min) followed by silica gel HPLC (column, YMC-Pack SIL SL12S16-1520WT; solvent, 40% EtOAc/hexane; flow rate, 8.0 mL min⁻¹; UV detection, 254 nm; retention time, 12.8 min).

4.3 Synthetic procedures

4.3.1 Synthesis of 2

To a solution of vibsanin A (26.3 mg, 65.3 μmol) in CH₂Cl₂ (540 μL) were added imidazole (20.9 mg, 0.305 mmol), DMAP (0.93 mg, 7.61 μmol), and *tert*-butyldimethylsilyl chloride (TBSCl, 44.5 mg, 0.296 mmol) at 0 °C under Ar atmosphere, and the reaction mixture was stirred for 1 h at the same temperature. EtOAc and H₂O were added to the mixture. The organic layer was separated and the water layer was extracted with EtOAc thrice. The combined organic layer was washed with brine, dried over Na₂SO₄, filtered, and concentrated *in vacuo*. The residue was purified by medium-pressure column chromatography (silica gel, 10–30% EtOAc/Hexane linear gradient) to afford **2** (24.0 mg, 46.3 μmol, 71%). [α]_D = +10.6° (*c* 2.36, CHCl₃, 18.6 °C). ¹H-NMR (500 MHz, 296 K, CDCl₃, 0.0096 M); δ 0.06 (3H, s, Si-CH₃), 0.07 (3H, s, Si-CH₃), 0.91 (9H, s, Si-C(CH₃)₃), 1.09 (3H, s, H-20), 1.12–1.19 (1H, m, H-5α), 1.25–1.33 (1H, m, H-12a), 1.42 (3H, s, H-19), 1.42–1.48 (1H, m, H-12b), 1.57 (3H, s, H-17), 1.66 (3H, s, H-16), 1.78 (1H, m, H-13a), 1.89 (3H, d, *J* = 1.2 Hz, H-5'), 1.91–1.98 (2H, m, H-1a, H-13b), 2.02 (1H, m, H-4α), 2.11–2.13 (1H, m, H-1b), 2.15 (3H, d, *J* = 1.2 Hz, H-4'), 2.19 (1H, m, H-4β), 2.28 (1H, m, H-5β), 2.76 (1H, dd, *J* = 11.7, 2.4 Hz, H-6), 3.99 (1H, d, *J* = 12.7 Hz, H-18a), 4.10 (1H, d, *J* = 12.7 Hz, H-18b), 5.05–5.08 (1H, t sep, *J* = 7.0, 1.4 Hz, H-14), 5.18 (1H, d, *J* = 10.0 Hz, H-8), 5.39 (1H, dd, *J* = 15.9, 10.0 Hz, H-9), 5.50 (1H, dd, *J* = 9.8, 6.9 Hz, H-2), 5.71 (1H, septet, *J* = 1.1 Hz, H-2'), 5.79 (1H, d, *J* = 15.9 Hz, H-10) ppm. ¹³C-NMR (126 MHz, 296 K, CDCl₃, 0.0096 M); δ -5.4 (Si-CH₃), -5.3 (Si-CH₃), 17.6 (C-17), 17.7 (C-19), 18.4 (Si-C), 20.2 (C-4'), 22.9 (C-4), 23.1 (C-20), 23.2 (C-13), 25.7 (C-16), 26.0 (C-3, Si-C(CH₃)₃), 26.3 (C-5), 27.4 (C-5'), 39.2 (C-12), 39.7 (C-11), 41.8 (C-1), 61.4 (C-7), 63.2 (C-6), 65.9 (C-18), 77.8 (C-8), 116.1 (C-2'), 119.2 (C-2), 120.8 (C-9), 124.7 (C-14), 131.2 (C-15), 141.3 (C-3), 147.0 (C-10), 156.9 (C-3'), 165.2 (C-1') ppm. HR-ESI-MS: *m/z* = 539.3535 ([M+Na]⁺, calcd. for C₃₁H₅₂O₄NaSi, 539.3533).

4.3.2 Synthesis of 3

To a solution of **2** (23.5 mg, 45.5 μmol) in MeOH (830 μL) and THF (830 μL) was added K₂CO₃ (33.9 mg, 0.246 mmol) under Ar atmosphere. The reaction mixture was stirred for 43 h at room temperature, then cooled to 0 °C, quenched with sat. NH₄Cl aq. (760 μL), and extracted with EtOAc. H₂O was added to the mixture, and the remaining organic layer was separated. The water layer was extracted with EtOAc thrice. The combined organic layer was washed with brine, dried over Na₂SO₄, filtered, and concentrated *in vacuo*. The residue was purified by open column chromatography (silica gel, 20–100% EtOAc/Hexane stepwise) to afford **3** (15.4 mg, 35.4 μmol, 78%). [α]_D = +4.08° (*c* 1.57, CHCl₃, 15.0 °C). ¹H-NMR (500 MHz, 296 K, CDCl₃, 0.014 M); δ 0.06 (3H, s, Si-CH₃), 0.07 (3H, s, Si-CH₃), 0.91 (9H, s, Si-C(CH₃)₃), 1.03–1.09 (1H, m, H-5α), 1.11 (3H, s, H-20), 1.25 (1H, s, OH), 1.29 (1H, ddd, *J* = 13.0, 12.3, 5.3 Hz, H-12a), 1.41 (3H, s, H-19), 1.44 (1H, ddd, *J* = 13.0, 12.6, 4.7 Hz, H-12b), 1.58 (3H, s, H-17), 1.67 (3H, s, H-16), 1.75–1.83 (2H, m, H-13a, OH), 1.93–2.02 (3H, m, H-1a, H-4α, H-13b), 2.13 (1H, dd, *J* = 12.5, 11.0 Hz, H-1b), 2.18 (1H, t, *J* = 12.0 Hz, H-4β), 2.20–2.28 (1H, m, H-5β), 2.79 (1H, dd, *J* = 11.7, 2.6 Hz, H-6), 3.99 (1H, d, *J* = 12.9 Hz, H-18a), 4.05 (1H, d, *J* = 9.6 Hz, H-8), 4.09 (1H, d, *J* = 12.9 Hz, H-18b), 5.07 (1H, br t, *J* = 7.1 Hz, H-14), 5.49 (1H, dd, *J* = 15.9, 9.6 Hz, H-9), 5.50 (1H, dd, *J* = 11.0, 6.4 Hz, H-2), 5.65 (1H, d, *J* = 15.9 Hz, H-10) ppm. ¹³C-NMR (126 MHz, 296 K, CDCl₃, 0.014 M); δ -5.3 (Si-CH₃), -5.3 (Si-CH₃), 16.9 (C-19), 17.7 (C-17), 18.4 (Si-C), 23.1 (C-4), 23.2 (C-13), 23.3 (C-20),

25.7 (C-16), 25.9 (3C, Si-C(CH₃)₃), 26.1 (C-5), 39.4 (C-11), 39.6 (C-12), 41.9 (C-1), 62.9 (C-7), 63.4 (C-6), 66.0 (C-18), 77.5 (C-8), 119.3 (C-2), 124.0 (C-9), 124.6 (C-14), 131.3 (C-15), 141.2 (C-3), 145.1 (C-10) ppm. HR-ESI-MS: *m/z* = 457.3126 ([M+Na]⁺, calcd. for C₂₆H₄₆O₃NaSi, 457.3114).

4.3.3 Synthesis of 4

To a suspension of NaH (60% dispersion in mineral oil) (23.4 mg, 0.585 mmol, washed with hexane) in DMF (650 μL) was added a solution of 3 (10.0 mg, 23.0 μmol) in DMF (3.0 mL) at 0 °C under Ar atmosphere. After stirring for 30 min at 0 °C, 1-bromo-3-methyl-2-butene (16.0 μL, 0.138 mmol) was added to the reaction mixture, and the mixture was stirred for 4 h at room temperature. The mixture was cooled to 0 °C, then DMF (2.2 mL), NaH (60% dispersion in mineral oil) (12.4 mg, 0.310 mmol), and 1-bromo-3-methyl-2-butene (10.5 μL, 0.091 mmol) were added. After stirring for 1.5 h at room temperature, the mixture was cooled to 0 °C, quenched with sat. NH₄Cl aq. (12 mL), and extracted with EtOAc. EtOAc and H₂O were added to the water layer, and the organic layer was separated. The water layer was extracted with EtOAc thrice. The combined organic layer was washed with brine, dried over Na₂SO₄, filtered, and concentrated *in vacuo*. The residue was purified by open column chromatography (silica gel, 5–20% EtOAc/Hexane stepwise) to afford 4 (4.9 mg, 9.7 μmol, 42%). [α]_D = +7.2° (c 0.36, CHCl₃, 18.8 °C). ¹H-NMR (500 MHz, 296 K, CDCl₃, 0.015 M); δ 0.06 (3H, s, Si-CH₃), 0.07 (3H, s, Si-CH₃), 0.91 (9H, s, Si-C(CH₃)₃), 1.03–1.08 (1H, m, H-5a), 1.11 (3H, s, H-20), 1.30 (1H, td, *J* = 12.5, 5.2 Hz, H-12a), 1.39 (3H, s, H-19), 1.44 (1H, td, *J* = 12.3, 4.5 Hz, H-12b), 1.58 (3H, s, H-17), 1.65 (3H, s, H-5'), 1.67 (3H, s, H-16), 1.73 (3H, s, H-4'), 1.75–1.83 (1H, m, H-13a), 1.95 (1H, dd, *J* = 12.8, 6.5 Hz, H-1α), 1.93–2.02 (2H, m, H-4a, H-13b), 2.14 (1H, dd, *J* = 12.3, 10.9 Hz, H-1β), 2.17–2.26 (2H, m, H-4b, H-5b), 2.79 (1H, dd, *J* = 11.2, 2.3 Hz, H-6), 3.64 (1H, d, *J* = 9.7 Hz, H-8), 3.95 (1H, dd, *J* = 11.4, 6.8 Hz, H-1'a), 4.01 (1H, dd, *J* = 11.4, 6.9 Hz, H-1'b), 4.00 (1H, d, *J* = 12.7 Hz, H-18), 4.09 (1H, d, *J* = 12.7 Hz, H-18b), 5.08 (1H, br t, *J* = 6.9 Hz, H-14), 5.36 (1H, m, H-2'), 5.41 (1H, dd, *J* = 16.0, 9.7 Hz, H-9), 5.50 (1H, dd, *J* = 10.1, 6.8 Hz, H-2), 5.61 (1H, d, *J* = 16.0 Hz, H-10) ppm. ¹³C-NMR (126 MHz, 296 K, CDCl₃, 0.015 M); δ -5.3 (Si-CH₃), -5.3 (Si-CH₃), 17.5 (C-19), 17.6 (C-17), 18.1 (C-5'), 18.4 (Si-C), 23.1 (C-4), 23.3 (C-13), 23.4 (C-20), 25.7 (C-16), 25.8 (C-4'), 26.0 (3C, Si-C(CH₃)₃), 26.2 (C-5), 39.4 (C-12), 39.7 (C-11), 41.8 (C-1), 62.0 (C-6), 62.3 (C-7), 65.1 (C-1'), 65.9 (C-18), 83.6 (C-8), 119.3 (C-2), 121.2 (C-2'), 123.1 (C-9), 124.7 (C-14), 131.3 (C-15), 136.6 (C-3'), 141.2 (C-3), 145.4 (C-10) ppm. HR-ESI-MS: *m/z* = 525.3749 ([M+Na]⁺, calcd. for C₃₁H₅₄O₃NaSi, 525.3740).

4.3.4 Synthesis of 1'-desoxovibsanin A (1)

To a solution of 4 (4.8 mg, 9.5 μmol) in THF (400 μL) was added 1.0 M tetra-*n*-butylammonium fluoride in THF (20.8 μL, 20.8 μmol) dropwise at 0 °C under Ar atmosphere. After stirring for 30 min at room temperature, EtOAc and H₂O were added to the reaction mixture, and the organic layer was separated. The water layer was extracted with EtOAc thrice. The combined organic layer was washed with brine, dried over Na₂SO₄, filtered, and concentrated *in vacuo*. The residue was purified by flash column chromatography (silica gel, 20–40% EtOAc/Hexane stepwise) to afford 1 (2.9 mg, 7.5 μmol, 80%), which was further purified by reversed-phase HPLC (column, YMC-Pack ODS-AMAM12S05-1520WT; solvent, 75% MeOH/H₂O; flow rate, 8.0 mL min⁻¹; UV detector, 220 nm and 254 nm; retention time, 82.4 min). [α]_D = +16.9° (c 0.33, CHCl₃, 21.5 °C). ¹H-NMR (500 MHz, 296 K, CDCl₃, 0.015 M); δ 1.05–1.09 (1H, m, H-5a), 1.12 (3H, s, H-20), 1.30 (1H, td, *J* = 12.2, 5.4 Hz, H-12a), 1.39 (3H, s, H-19), 1.46 (1H, td, *J* = 13.0, 4.6 Hz, H-12b), 1.58 (3H, s, H-17), 1.65 (3H, s, H-5'), 1.68 (3H, s, H-16), 1.73 (3H, s, H-4'), 1.75–1.83 (1H, m, H-13a), 1.96 (1H, dd, *J* = 12.7, 6.6 Hz, H-1α), 1.94–2.05 (2H, m, H-4a, H-13b), 2.16 (1H, dd, *J* = 12.5, 10.6 Hz, H-1β), 2.14–2.29 (2H, m, H-4b, H-5b), 2.71 (1H, dd, *J* = 11.9, 2.4 Hz, H-6), 3.64 (1H, d, *J* = 9.7 Hz, H-8), 3.96 (1H, dd, *J* = 11.4, 6.8 Hz, H-1'a), 4.01 (1H, dd, *J* = 11.4, 6.9 Hz, H-1'b), 4.02 (1H, br d, *J* = 12.6 Hz, H-18a), 4.20 (1H, br dd, *J* = 12.6, 3.0 Hz, H-18b), 5.07–5.10 (1H, t sep, *J* = 7.0, 1.3 Hz,

H-14), 5.37 (1H, t sep, $J = 6.9, 1.3$ Hz, H-2'), 5.42 (1H, dd, $J = 16.0, 9.7$ Hz, H-9), 5.53 (1H, dd, $J = 10.0, 6.7$ Hz, H-2), 5.61 (1H, d, $J = 16.0$ Hz, H-10) ppm. ^{13}C -NMR (126 MHz, 296 K, CDCl_3 , 0.015 M); δ 17.5 (C-19), 17.6 (C-17), 18.1 (C-5'), 23.1 (C-4), 23.3 (C-13), 23.4 (C-20), 25.7 (C-16), 25.8 (C-4'), 26.2 (C-5), 39.5 (C-12), 39.8 (C-11), 42.0 (C-1), 62.0 (C-6), 62.2 (C-7), 65.1 (C-1'), 66.1 (C-18), 83.6 (C-8), 120.9 (C-2), 121.2 (C-2'), 123.4 (C-9), 124.6 (C-14), 131.4 (C-15), 136.6 (C-3'), 141.6 (C-3), 145.0 (C-10) ppm. HR-ESI-MS: $m/z = 411.2881$ ($[\text{M}+\text{Na}]^+$, calcd. for $\text{C}_{25}\text{H}_{40}\text{O}_3\text{Na}$, 411.2875).

4.4 Inhibition of specific binding of [^3H]PDBu to the recombinant PKCs and synthetic PKC C1 peptides

The binding of compounds to PKC α , PKC δ , α -C1A (72-mer), α -C1B (72-mer), δ -C1A, and δ -C1B peptides was evaluated by the procedure of Sharkey and Blumberg²² with modifications as reported previously²⁴ using 50 mM Tris-maleate buffer (pH 7.39 at 4 °C; containing 0.1 mM CaCl_2 for the recombinant PKC α), 11.4 nM (for PKC α), 11.6 nM (for PKC δ), 13.8 nM (for δ -C1B), 20 or 40 nM (for α -C1B), or 40 nM (α -C1A, and δ -C1A) receptors, 10 nM (for the recombinant proteins) or 20 nM (for the C1 peptides) [^3H]PDBu (17.16 Ci mmol $^{-1}$), 50 $\mu\text{g mL}^{-1}$ 1,2-dioleoyl-*sn*-glycero-3-phospho-L-serine, 3 mg mL $^{-1}$ bovine γ -globulin, and increasing concentrations of the unlabeled ligands.

The assay tubes containing 250 μL of mixture solution were incubated at 37 °C for 10 min and then at 4 °C (on ice) for 10 min for the recombinant proteins, at 25 °C for 10 min and then at 4 °C (on ice) for 10 min for α -C1A and δ -C1B, or at 4 °C (on ice) for 30 min for α -C1B and δ -C1A, after which 187 μL of 30% poly(ethylene glycol) (PEG) 8000 was added. The tubes were vortexed and centrifuged at 12,000 rpm for 10 min at 4 °C. A 50 μL aliquot of the supernatant of the total- and nonspecific binding groups was transferred to a scintillation vial, and its radioactivity was measured to determine the free [^3H]PDBu concentration. The remainder of the supernatant of each tube was removed by aspiration. The tips of the tubes were cut off, and the radioactivity in the pellets was measured to determine the bound [^3H]PDBu. Specific binding represents the difference between the total and nonspecific binding. The supernatant and pellet vials were immersed in 2 mL of scintillation cocktail (Insta-Gel Plus, PerkinElmer, Waltham, MA). In each experiment, triplicate measurements at each concentration of ligand were performed.

Binding affinity was evaluated based on the total ligand concentration required to cause 50% inhibition of the specific binding of [^3H]PDBu, IC_{50} . The following values were used for the calculation of the binding inhibition constant, K_i ; K_d , a dissociation constant of [^3H]PDBu for each peptide; k , a partition coefficient of [^3H]PDBu between supernatant and γ -globulin/phosphatidylserine pellet; $[L_T]$, the total concentration of [^3H]PDBu in the assay solution determined from total radioactive counts; $[RL_0]$, a specifically-bound concentration of [^3H]PDBu in the absence of unlabeled ligands; $[RL]$, a specifically-bound concentration of [^3H]PDBu in the presence of unlabeled ligands which was calculated as $[RL] = [^3\text{H in pellet}] - k \times ([L_T] - [^3\text{H in pellet}])$; $[L_0]$, a free concentration of [^3H]PDBu in the absence of unlabeled ligands; $[L_{50}]$, a free concentration of [^3H]PDBu at 50% inhibition which was calculated as $[L_{50}] = ([L_T] - [RL_0]/2)/(1 + k)$. The smaller values (15.15, 14.74, or 13.92 Ci mmol $^{-1}$) of the specific activity of [^3H]PDBu were used for the calculation in consideration of radioactive decay. Two or three independent experiments for each combination of ligands and the C1 peptides with three concentrations of unlabeled ligands in $10^{0.5}$ M increments across the IC_{50} point were performed.

The logarithmic concentration of the unlabeled ligand, $\log_{10}[I]$ (M), on the horizontal axis was plotted versus $\ln[\theta/(1 - \theta)]$ on the vertical axis. $\theta = [RL]/[RL_0]$, a ratio of specific [^3H]PDBu binding to that of the total binding group. Linear regression was performed using the least-squares method, and the IC_{50} value was defined as the concentration at which the regression line intersected the horizontal axis ($\ln[\theta/(1 - \theta)] = 0$).

The binding inhibition constant, K_i , of VibA for δ -C1B was calculated by the Munson-Rodbard equa-

tion,³⁹

$$K_i = \frac{IC_{50}}{1 + \frac{[L_T](y_0+2)}{2K_d(y_0+1)} + y_0} - K_d \left(\frac{y_0}{y_0 + 2} \right),$$

where $y_0 = [RL_0]/[L_0]$.

In the other cases, K_i values were calculated by the Goldstein–Barrett equation,⁴⁰

$$K_i = \frac{[I_{50}]}{2 \frac{[L_{50}]}{[L_0]} - 1 + \frac{[L_{50}]}{K_d}},$$

where $[I_{50}]$ is a free concentration of unlabeled ligands at 50% inhibition and approximated by the IC_{50} value.

The mean K_i values and the 95% confidence intervals (based on t -distribution) were calculated on the logarithm scale and converted to the nanomolar unit.

From the binding assay for the recombinant proteins, the K_i values for each of two binding sites were estimated by nonlinear regression to the equation,

$$\theta = \frac{1}{[RL]_0} \frac{[R_T] ([L_T] - \theta[RL]_0)}{\left(\frac{1}{\left(1 + \frac{[I]}{K_{i-C1A}}\right) K_{d-C1A} + ([L_T] - \theta[RL]_0)} + \frac{1}{\left(1 + \frac{[I]}{K_{i-C1B}}\right) K_{d-C1B} + ([L_T] - \theta[RL]_0)} \right)},$$

where θ is a [³H]PDBu binding ratio, $[RL]_0$ is a bound [³H]PDBu concentration in the absence of VibA, $[R_T]$ is a total effective concentration of the protein estimated from $[RL]_0$ and the K_d values, $[L_T]$ is a total concentration of [³H]PDBu, $[I]$ is a free concentration of the unlabeled ligand and approximated by the equation $[I] = [I_T] - 1.1 \times [RL]_0(1 - \theta)$, K_d is a dissociation constant of [³H]PDBu (the K_d values used for the α -C1A,²⁴ α -C1B,²⁴ δ -C1A,⁴¹ and δ -C1B⁴¹ domains were 1.1, 5.3, 2.04, and 0.33 nM, respectively), and K_i is a binding inhibition constant of VibA and a fitting parameter. In the nonlinear regression analysis, we assumed that K_i for α -C1A < K_i for α -C1B and K_i for δ -C1A > K_i for δ -C1B.

4.5 Molecular modeling

Three-dimensional structures of VibA and **1** were created by the Avogadro (version 1.2.0) software.⁴²

Homology modeling of the human PKC α -C1A domain were performed by the MODELLER software⁴³ (version 9.23). 1PTR.pdb¹⁴ (PKC δ -C1B domain in complex with phorbol 13-acetate), 4L9M.pdb⁴⁴ (RasGRP1), and 3CXL.pdb⁴⁵ (α -chimaerin) were used as multiple templates. Phorbol-13-acetate from 1PTR and zinc ions from all templates were included in the modeling. The distances between the zinc ions and the zinc-coordinated sulfur atoms (2.3 Å), and between zinc ions and the zinc-coordinated nitrogen atoms (2.0 Å) were all restrained with a Gaussian function with standard deviation values of 0.2. Each model was first optimized with the variable target function method (VTFM; autosched.slow, max_var_ iterations = 500) with conjugate gradients (CG), and was then refined using molecular dynamics (MD; md_level = refine.very_slow) with simulated annealing (SA). The created fifty models were assessed by the DOPE score.

Docking and molecular dynamics simulations and MM-PBSA calculation were performed as previously described.³¹ Amber ff14SB,⁴⁶ ZAFF,⁴⁷ LIPID17, GAFF2 (with AM1-BCC charge) force fields were used for the MD simulation. The decomposition of energies per residue was performed using the MMPBSA.py.MPI module⁴⁸ in the AmberTools 20 and 21 packages.^{49,50}

The following programs and servers were used for the calculation and analysis: The MODELLER (version 9.23) software, the AutoDock GPU (version 4.2.6) program,^{51,52} the PPM server and program,³⁵ the CHARMM-GUI server,⁵³⁻⁵⁵ Antechamber,⁵⁶ tleap, and MMPBSA.py.MPI⁴⁸ modules in the AmberTools 20 and 21 packages,^{49,50} the GROMACS (version 2021.1) program,⁵⁷ and the PyMOL program.⁵⁸

4.6 Cell growth inhibition assay

MOLT-4F human leukemia cell line was purchased from RIKEN Cell Bank in Japan (RCB1936) and grown in RPMI-1640 medium with 10% heat-inactivated fetal bovine serum (FBS), 100 IU/mL penicillin, and 100 µg/mL streptomycin in a 5% CO₂ humidified incubator at 37 °C.

Test compounds were dissolved in DMSO, and the DMSO stock was diluted with the medium. MOLT-4F cells were seeded in 96-well plates at a density of 5×10^3 cells/well in 95 µL of the medium, and then 5 µL solution of each compound was added (final DMSO concentration of 0.5%). After 48 h incubation, 10 µL of Cell Counting Kit-8 was added to each well, and the plate was incubated at 37 °C for a further 4 h. Absorbances for the control well (*C*) and test well (*T*) were measured at 450 nm, together with the absorbance at time 0 (*C*₀). A blank value was subtracted from each value. Cell growth (% of control) was expressed as $100 \times [(T - C_0)/(C - C_0)]$ ($T \geq C_0$) or $100 \times [(T - C_0)/C_0]$ ($T < C_0$). Two or three independent experiments with a triplicate setting were performed. The GI₅₀ was calculated from the linear regression to two concentrations across 50% growth inhibition on the logarithm scale and converted to the molar unit.

4.7 Stability test

Ten millimolar solution of VibA or **1** in DMSO (4 or 5 µL) was diluted 100-fold by phosphate-buffered saline [Dulbecco's formula (modified) without magnesium and calcium ions, pH 7.4, TaKaRa, Japan]. The final concentration of the compounds was 0.1 mM. Test solutions were incubated at 37 °C, from which 50 µL was sampled at 0, 2, 4, 6, and 24 h for VibA, and 0, 2, 4, 8, and 24 h for **1**. For each time point, duplicate set was used. After sampling, each sample was frozen. Just before HPLC analysis, each sample was thawed by adding 450 µL of ice-cold MeOH and filtered by a membrane filter. Then, 300 µL of each sample was analyzed using HPLC (column, YMC-Pack ODS-A AA12S05-1006WT; solvent, 85% MeOH/H₂O; flow rate, 2.0 mL min⁻¹; UV detection, 220 nm; retention time, 4.7 min for VibA and 5.3 min for **1**). The remaining amount of the compounds was estimated by integrating the peak areas in the HPLC chromatograms.

The half-lives *t* were determined from the nonlinear regression to the equation $A = A_0 \left(\frac{1}{2}\right)^{\frac{t}{T}}$, where *A* is peak area at $\lambda = 220$ nm at given time *t* (h), *A*₀ is peak area at 0 h, *T* is the half-life in h. The nonlinear regression analysis was conducted using the R software (version 4.1.0).

For the LC-TOF-MS analysis, 10 mM solution of VibA in DMSO (1 µL) was diluted 100 fold by phosphate-buffered saline. The solution was incubated at 37 °C for 24 h, from which 50 µL was sampled and frozen. The sample was thawed by adding 50 µL of ice-cold MeOH, filtered by a membrane filter, and then analyzed by an LC-TOF-MS system (C18 column; linear gradient from 30% to 100% MeOH/H₂O in 8 min).

Declaration of Competing Interest

The authors declare that they have no known competing financial interests or personal relationships that could have appeared to influence the work reported in this paper.

ACKNOWLEDGEMENTS

This work was supported by JSPS KAKENHI Grant numbers 19K05846 (to R.C.Y.) and 17H06405 (to K.I. and R.C.Y.).

References

- [1] Yasutomi Nishizuka. The role of protein kinase C in cell surface signal transduction and tumour promotion. *Nature*, 308:693–698, 1984.
- [2] Yasutomi Nishizuka. Protein kinase C and lipid signaling for sustained cellular responses. *The FASEB Journal*, 9(7):484–496, 1995.
- [3] Alexandra C. Newton. Protein kinase C as a tumor suppressor. *Seminar in Cancer Biology*, 48(March 2017):18–26, 2018.
- [4] Paul A. Wender, Vishal A. Verma, Thomas J. Paxton, and Thomas H. Pillow. Function-Oriented Synthesis, Step Economy, and Drug Design. *Accounts of Chemical Research*, 41(1):40–49, jan 2008.
- [5] Lisa L. Gallegos and Alexandra C. Newton. Spatiotemporal dynamics of lipid signaling: protein kinase C as a paradigm. *IUBMB Life*, 60(12):782–789, 2008.
- [6] Kazuhiro Irie and Ryo C. Yanagita. Synthesis and biological activities of simplified analogs of the natural PKC ligands, bryostatin-1 and aplysiatoxin. *Chemical Record*, 14(2):251–267, apr 2014.
- [7] Mark Lebwohl, Neil Swanson, Lawrence L. Anderson, Anita Melgaard, Zhenyi Xu, and Brian Berman. Ingenol Mebutate Gel for Actinic Keratosis. *New England Journal of Medicine*, 366(11):1010–1019, 2012.
- [8] Jason K. Cullen, Glen M. Boyle, Pei Yi Yap, Stefan Elmlinger, Jacinta L. Simmons, Natasa Broit, Jenny Johns, Blake Ferguson, Lidia A. Maslovskaya, Andrei I. Savchenko, Paul Malek Mirzayans, Achim Porzelle, Paul V. Bernhardt, Victoria A. Gordon, Paul W. Reddell, Alberto Pagani, Giovanni Appendino, Peter G. Parsons, and Craig M. Williams. Activation of PKC supports the anticancer activity of tigilanol tiglate and related epoxytigilanes. *Scientific Reports*, 11(1):1–14, 2021.
- [9] Kazuyoshi Kawazu. Isolation of Vibsanines A, B, C, D, E and F from *Viburnum odoratissimum*. *Agricultural and Biological Chemistry*, 44(6):1367–1372, 1980.
- [10] Yoshiyasu Fukuyama, Miwa Kubo, Tomoyuki Esumi, Kenichi Harada, and Hideaki Hioki. Chemistry and Biological Activities of Vibsanine-Type Diterpenoids. *Heterocycles*, 81(7):1571, 2010.
- [11] Miwa Kubo, Megumi Nakai, Kenichi Harada, and Yoshiyasu Fukuyama. Structure of seven new vibsanine-type diterpenoids from *Viburnum awabuki*. *Tetrahedron*, 75(16):2379–2384, 2019.
- [12] Zu Yin Yu, He Xiao, Li Mei Wang, Xing Shen, Yu Jing, Lin Wang, Wen Feng Sun, Yan Feng Zhang, Yu Cui, Ya Jun Shan, Wen Bing Zhou, Shuang Xing, Guo Lin Xiong, Xiao Lan Liu, Bo Dong, Jian Nan Feng, Li Sheng Wang, Qing Liang Luo, Qin Shi Zhao, and Yu Wen Cong. Natural product vibsanin A induces differentiation of myeloid leukemia cells through PKC activation. *Cancer Research*, 76(9):2698–2709, 2016.
- [13] Wataru Matsuki, So Miyazaki, Keisuke Yoshida, Akihiro Ogura, Yukiko Sasazawa, Ken-ichi Takao, and Siro Simizu. Synthesis and evaluation of biological activities of vibsanin A analogs. *Bioorganic and Medicinal Chemistry Letters*, 27(19):4536–4539, 2017.
- [14] Gongyi Zhang, Marcelo G. Kazanietz, Peter M. Blumberg, and James H. Hurley. Crystal structure of the Cys2 activator-binding domain of protein kinase C δ in complex with phorbol ester. *Cell*, 81(6):917–924, 1995.
- [15] Y. Pak, I. J. Enyedy, J. Varady, J. W. Kung, P. S. Lorenzo, P. M. Blumberg, and S. Wang. Structural basis of binding of high-affinity ligands to protein kinase C: Prediction of the binding modes through a new molecular dynamics method and evaluation by site-directed mutagenesis. *Journal of Medicinal Chemistry*, 44(11):1690–1701, 2001.

- [16] Yasuyuki Endo, Shunji Takehana, Michihiro Ohno, Paul E. Driedger, Silvia Stabel, Miho Y. Mizutani, Nobuo Tomioka, Akiko Itai, and Koichi Shudo. Clarification of the binding mode of teleocidin and benzolactams to the Cys2 domain of protein kinase C δ by synthesis of hydrophobically modified, teleocidin-mimicking benzolactams and computational docking simulation. *Journal of Medicinal Chemistry*, 41(9):1476–1496, 1998.
- [17] Yoshiki Ashida, Ryo C. Yanagita, Chise Takahashi, Yasuhiro Kawanami, and Kazuhiro Irie. Binding mode prediction of aplysiatoxin, a potent agonist of protein kinase C, through molecular simulation and structure–activity study on simplified analogs of the receptor-recognition domain. *Bioorganic and Medicinal Chemistry*, 24(18):4218–4227, 2016.
- [18] Juan He, Li Yan Peng, Lin Tu, Xing De Wu, Liao Bing Dong, Zheng Hong Pan, Xuan Qin Chen, Jia Su, Yu Zhao, Gang Xu, Xiao Cheng, Yan Li, and Qin Shi Zhao. Vibsane-type diterpenes from leaves and twigs of *Viburnum odoratissimum*. *Fitoterapia*, 109:224–229, 2016.
- [19] Yoshiyasu Fukuyama, Hiroyuki Minami, Shigeru Takaoka, Mitsuki Kodama, Kazuyoshi Kawazu, and Hisao Nemoto. Absolute structure of vibsanins B and C, and their chemical correlation. *Tetrahedron Letters*, 38(8):1435–1438, 1997.
- [20] Mitsunori Ono, Yumiko Wada, Naoto Yamaguchi, and Jifeng Duan. Epoxyvibsantin B, 2002.
- [21] Yusuke Hanaki, Yuki Shikata, Masayuki Kikumori, Natsuki Hotta, Masaya Imoto, and Kazuhiro Irie. Identification of protein kinase C isozymes involved in the anti-proliferative and pro-apoptotic activities of 10-Methyl-aplog-1, a simplified analog of debromoaplysiatoxin, in several cancer cell lines. *Biochemical and Biophysical Research Communications*, 495(1):438–445, 2018.
- [22] Nancy A. Sharkey and Peter M. Blumberg. Highly lipophilic phorbol esters as inhibitors of specific [3H]phorbol 12,13-dibutyrate binding. *Cancer Research*, 45:19–24, 1985.
- [23] Kazuhiro Irie, Kentaro Oie, Akifumi Nakahara, Yoshiaki Yanai, Hajime Ohigashi, Paul A. Wender, Hiroyuki Fukuda, Hiroaki Konishi, and Ushio Kikkawa. Molecular basis for protein kinase C isozyme-selective binding: The synthesis, folding, and phorbol ester binding of the cysteine-rich domains of all protein kinase C isozymes. *Journal of the American Chemical Society*, 120(36):9159–9167, 1998.
- [24] Mayumi Shindo, Kazuhiro Irie, Akifumi Nakahara, Hajime Ohigashi, Hiroaki Konishi, Ushio Kikkawa, Hiroyuki Fukuda, and Paul A. Wender. Toward the identification of selective modulators of protein kinase C (PKC) isozymes: Establishment of a binding assay for PKC isozymes using synthetic C1 peptide receptors and identification of the critical residues involved in the phorbol ester binding. *Bioorganic and Medicinal Chemistry*, 9(8):2073–2081, 2001.
- [25] Ryo C. Yanagita, Hiroaki Kamachi, Keisuke Tanaka, Akira Murakami, Yu Nakagawa, Harukuni Tokuda, Hiroshi Nagai, and Kazuhiro Irie. Role of the phenolic hydroxyl group in the biological activities of simplified analogue of aplysiatoxin with antiproliferative activity. *Bioorganic and Medicinal Chemistry Letters*, 20(20):6064–6066, 2010.
- [26] Ryo C. Yanagita, Yu Nakagawa, Nobuhiro Yamanaka, Kaori Kashiwagi, Naoaki Saito, and Kazuhiro Irie. Synthesis, conformational analysis, and biological evaluation of 1-hexylindolactam-V10 as a selective activator for novel protein kinase C isozymes. *Journal of Medicinal Chemistry*, 51(1):46–56, 2008.
- [27] Yu Nakagawa, Kazuhiro Irie, Yusuke Komiya, Hajime Ohigashi, and Ken-ichiro Tsuda. Synthesis, conformation and PKC isozyme surrogate binding of indolinolactam-Vs, new conformationally restricted analogues of (–)-indolactam-V. *Tetrahedron*, 60(33):7077–7084, 2004.
- [28] Yu Nakagawa, Kazuhiro Irie, Ryo C. Yanagita, Hajime Ohigashi, Ken-ichiro Tsuda, Kaori Kashiwagi, and Naoaki Saito. Design and synthesis of 8-octyl-benzolactam-V9, a selective activator for protein kinase C ϵ and η . *Journal of Medicinal Chemistry*, 49(9):2681–2688, 2006.

- [29] D. E. Macfarlane and L. Manzel. Activation of β -isozyme of protein kinase C (PKC β) is necessary and sufficient for phorbol ester-induced differentiation of HL-60 promyelocytes. Studies with PKC β -defective pet mutant. *Journal of Biological Chemistry*, 269(6):4327–4331, 1994.
- [30] Ji Hye Kang, Megan L. Peach, Yongmei Pu, Nancy E. Lewin, Marc C. Nicklaus, Peter M. Blumberg, and Victor E. Marquez. Conformationally constrained analogues of diacylglycerol (DAG). 25. Exploration of the *sn*-1 and *sn*-2 carbonyl functionality reveals the essential role of the *sn*-1 carbonyl at the lipid interface in the binding of DAG-lactones to protein kinase C. *Journal of Medicinal Chemistry*, 48(18):5738–5748, 2005.
- [31] Atsuko Gonda, Koji Takada, Ryo C Yanagita, Shingo Dan, and Kazuhiro Irie. Effects of side chain length of 10-methyl-aplog-1, a simplified analog of debromoaplysiatoxin, on PKC binding, anti-proliferative, and pro-inflammatory activities. *Bioscience, Biotechnology, and Biochemistry*, 85(1):168–180, 2021.
- [32] Dina M. Sigano, Megan L. Peach, Kassoum Nacro, Yongseok Choi, Nancy E. Lewin, Marc C. Nicklaus, Peter M. Blumberg, and Victor E. Marquez. Differential Binding Modes of Diacylglycerol (DAG) and DAG Lactones to Protein Kinase C (PK-C). *Journal of Medicinal Chemistry*, 46:1571–1579, 2003.
- [33] Scott Horowitz and Raymond C. Trievel. Carbon-oxygen hydrogen bonding in biological structure and function. *Journal of Biological Chemistry*, 287(50):41576–41582, 2012.
- [34] Isabel Rozas, Ibon Alkorta, and José Elguero. Bifurcated hydrogen bonds: Three-centered interactions. *Journal of Physical Chemistry A*, 102(48):9925–9932, 1998.
- [35] Mikhail A. Lomize, Irina D. Pogozheva, Hyeon Joo, Henry I. Mosberg, and Andrei L. Lomize. OPM database and PPM web server: Resources for positioning of proteins in membranes. *Nucleic Acids Research*, 40(D1):D370–D376, 2012.
- [36] H. G. Drexler, G. Gaedicke, and J. Minowada. T-leukemia cell lines CCRF-CEM, HPB-ALL, JM and MOLT-4: Changes in isoenzyme profiles during induction of differentiation. *Blut*, 54(2):79–87, 1987.
- [37] Takumi Kobayashi, Ryo C. Yanagita, and Kazuhiro Irie. Synthesis and biological activities of simplified aplysiatoxin analogs focused on the CH/ π interaction. *Bioorganic and Medicinal Chemistry Letters*, 30(24):127657, 2020.
- [38] Yu Nakagawa, Kazuhiro Irie, Ryo C. Yanagita, Hajime Ohigashi, and Ken-ichiro Tsuda. Indolactam-V is involved in the CH/ π interaction with Pro-11 of the PKC δ C1B domain: application for the structural optimization of the PKC δ ligand. *Journal of the American Chemical Society*, 127(16):5746–5747, 2005.
- [39] Peter J. Munson and David Rodbard. An Exact Correction to the “Cheng-Prusoff” Correction. *Journal of Receptor Research*, 8(1–4):533–546, 1988.
- [40] A. Goldstein and Ronald W. Barrett. Ligand dissociation constants from competition binding assays: errors associated with ligand depletion. *Molecular Pharmacology*, 31(6):603–609, 1987.
- [41] Yongmei Pu, Susan H. Garfield, Noemi Kedei, and Peter M. Blumberg. Characterization of the differential roles of the twin C1a and C1b domains of protein kinase C δ . *Journal of Biological Chemistry*, 284(2):1302–1312, 2009.
- [42] Marcus D. Hanwell, Donald E. Curtis, David C. Lonie, Tim Vandermeersch, Eva Zurek, and Geoffrey R. Hutchison. Avogadro: an advanced semantic chemical editor, visualization, and analysis platform. *Journal of Cheminformatics*, 4:17, 2012.
- [43] Benjamin Webb and Andrej Sali. Comparative Protein Structure Modeling Using MODELLER. *Current protocols in bioinformatics*, 54:5.6.1–5.6.37, 2016.

- [44] Jeffrey S. Iwig, Yvonne Vercoulen, Rahul Das, Tiago Barros, Andre Limnander, Yan Che, Jeffrey G. Pelton, David E. Wemmer, Jeroen P. Roose, and John Kuriyan. Structural analysis of autoinhibition in the Ras-specific exchange factor RasGRP1. *eLife*, 2:e00813, 2013.
- [45] L. Shen, M. Buck, Y. Tong, W. Tempel, F. MacKenzie, C. H. Arrowsmith, A. M. Edwards, C. Bountra, M. Wilkstrom, A. Bochkarev, H. Park, and Structural Genomics Consortium (SGC). Crystal structure of human chimerin 1 (CHN1). 2008.
- [46] James A. Maier, Carmenza Martinez, Koushik Kasavajhala, Lauren Wickstrom, Kevin E. Hauser, and Carlos Simmerling. ff14SB: Improving the Accuracy of Protein Side Chain and Backbone Parameters from ff99SB. *Journal of Chemical Theory and Computation*, 11(8):3696–3713, 2015.
- [47] Martin B. Peters, Yue Yang, Bing Wang, László Füsti-Molnár, Michael N. Weaver, and Kenneth M. Merz. Structural survey of zinc-containing proteins and development of the zinc AMBER force field (ZAFF). *Journal of Chemical Theory and Computation*, 6(9):2935–2947, 2010.
- [48] Bill R. Miller, III, T. Dwight McGee, Jr., Jason M. Swails, Nadine Homeyer, Holger Gohlke, and Adrian E. Roitberg. MMPBSA.py : An Efficient Program for End-State Free Energy Calculations. *Journal of Chemical Theory and Computation*, 8:3314–3321, 2012.
- [49] D. A. Case, K. Belfon, I. Y. Ben-Shalom, S. R. Brozell, D. S. Cerutti, T. E. Cheatham, III, V. W. D. Cruzeiro, T. A. Darden, R. E. Duke, G. Giambasu, M. K. Gilson, H. Gohlke, A. W. Goetz, R. Harris, S. Izadi, S. A. Izmailov, K. Kasavajhala, A. Kovalenko, R. T. Krasny, T. Kurtzman, T. S. Lee, S. LeGrand, P. Li, C. Lin, J. Liu, T. Luchko, R. Luo, V. Man, K. M. Merz, Y. Miao, O. Mikhailovskii, G. Monard, H. Nguyen, A. Onufriev, F. Pan, S. Pantano, R. Qi, D. R. Roe, A. Roitberg, C. Sagui, S. Schott-Verdugo, J. Shen, C. Simmerling, N. R. Skrynnikov, J. Smith, J. Swails, R. C. Walker, J. Wang, L. Wilson, R. M. Wolf, X. Wu, Y. Xiong, Y. Xue, D. M. York, and P. A. Kollman. AMBER2020, 2020.
- [50] D. A. Case, H. M. Aktulga, K. Belfon, I. Y. Ben-Shalom, S. R. Brozell, D. S. Cerutti, T. E. Cheatham, III, G. A. Cisneros, V. W. D. Cruzeiro, T. A. Darden, R. E. Duke, G. Giambasu, M. K. Gilson, H. Gohlke, A. W. Goetz, R. Harris, S. Izadi, S. A. Izmailov, K. Kasavajhala, M. C. Kaymark, E. King, A. Kovalenko, T. Kurtzman, T. S. Lee, S. LeGrand, P. Li, C. Lin, J. Liu, T. Luchko, R. Luo, M. Machado, V. Man, M. Manathunga, K. M. Merz, Y. Miao, O. Mikhailovskii, G. Monard, H. Nguyen, K. A. O’Hearn, A. Onufriev, F. Pan, S. Pantano, R. Qi, A. Rahnamoun, D. R. Roe, A. Roitberg, C. Sagui, S. Schott-Verdugo, J. Shen, C. Simmerling, N. R. Skrynnikov, J. Smith, J. Swails, R. C. Walker, J. Wang, H. Wei, R. M. Wolf, X. Wu, Y. Xue, D. M. York, S. Zhao, and P. A. Kollman. AMBER2021, 2021.
- [51] Garrett M. Morris, Ruth Huey, William Lindstrom, Michel F. Sanner, Richard K. Belew, David S. Goodsell, and Arthur J. Olson. AutoDock4 and AutoDockTools4: Automated Docking with Selective Receptor Flexibility. *Journal of Computational Chemistry*, 30(16):2785–2791, 2009.
- [52] Diogo Santos-Martins, Leonardo Solis-Vasquez, Andreas F. Tillack, Michel F. Sanner, Andreas Koch, and Stefano Forli. Accelerating AutoDock4 with GPUs and Gradient-Based Local Search. *Journal of Chemical Theory and Computation*, 17:1060–1073, 2021.
- [53] Sunhwan Jo, Taehoon Kim, Vidyashankara G. Iyer, and Wonpil Im. CHARMM-GUI: A Web-based Graphical User Interface for CHARMM. *Journal of Computational Chemistry*, 29:1859–1865, 2008.
- [54] Jumin Lee, Xi Cheng, Jason M. Swails, Min Sun Yeom, Peter K. Eastman, Justin A. Lemkul, Shuai Wei, Joshua Buckner, Jong Cheol Jeong, Yifei Qi, Sunhwan Jo, Vijay S. Pande, David A. Case, Charles L. Brooks, Alexander D. MacKerell, Jeffery B. Klauda, and Wonpil Im. CHARMM-GUI Input Generator for NAMD, GROMACS, AMBER, OpenMM, and CHARMM/OpenMM Simulations Using the CHARMM36 Additive Force Field. *Journal of Chemical Theory and Computation*, 12(1):405–413, 2016.

- [55] Sunhwan Jo, Taehoon Kim, and Wonpil Im. Automated builder and database of protein/membrane complexes for molecular dynamics simulations. *PLoS ONE*, 2(9):e880, 2007.
- [56] Junmei Wang, Wei Wang, Peter A. Kollman, and David A. Case. Automatic atom type and bond type perception in molecular mechanical calculations. *Journal of Molecular Graphics and Modelling*, 25(2):247–260, 2006.
- [57] Mark James Abraham, Teemu Murtola, Roland Schulz, Szilárd Páll, Jeremy C. Smith, Berk Hess, and Erik Lindah. Gromacs: High performance molecular simulations through multi-level parallelism from laptops to supercomputers. *SoftwareX*, 1-2:19–25, 2015.
- [58] The PyMOL Molecular Graphics System, Schrödinger, LLC.